Interleaved DC/DC Boost Converter with Coupled Inductors

Slavomir KASCAK, Michal PRAZENICA, Miriam JARABICOVA, Marek PASKALA

Department of Mechatronics and Electronics, Faculty of Electrical Engineering,
University of Zilina, Univerzitna 1, 010 26 Zilina, Slovakia

slavomir.kascak@fel.uniza.sk, michal.prazenica@fel.uniza.sk,
miriam.jarabicova@fel.uniza.sk, marek.paskala@fel.uniza.sk

DOI: 10.15598/aeee.v16i2.2413

Abstract. *This paper deals with the analysis of boost interleaved DC-DC converter with a coupled inductor on the same magnetic core. The advantage of the coupled inductor over the non-coupled case is investigated. The ripple current equations as an input current for the boost operation mode and the ripple current in individual phase of the interleaved converter using coupled inductor are explained analytically, supported by simulation and experimental results. The novelty of the paper is an investigation of current ripples of interleaved boost converter operated over 50 % of duty ratio and utilization of the converter in the application of electrically driven vehicle.*

Keywords

Bidirectional converter, coupling coefficient, coupled inductor.

1. Introduction

Nowadays, the interleaved topologies are widely used due to their advantageous properties, such as lowered current ripple and volume reduction [1], [2], [3], [4], [5], [6], [7], [8] and [9].

For higher power applications, there are more possibilities how to perform higher power density regarding the efficiency of the converter. The first choice is to utilize of the paralleling of power switches, as shown in Fig. 1. This converter includes only one inductor and two half-bridge legs connected in parallel. This is done for reasons of obtaining higher current ratings, thermal improvements, and sometimes for redundancy. If losses are not equally shared, the thermal differences among the devices will lead to other problems and possible failure of the transistors. Therefore, the thermal coefficient of the Collector-Emitter Voltage $V_{CE(SAT)}$ is an important parameter when paralleling IGBTs. It must be positive to allow current sharing. On the other hand, the higher positive thermal coefficient, the higher losses arise, because at high temperature the $V_{CE(SAT)}$ is increased.

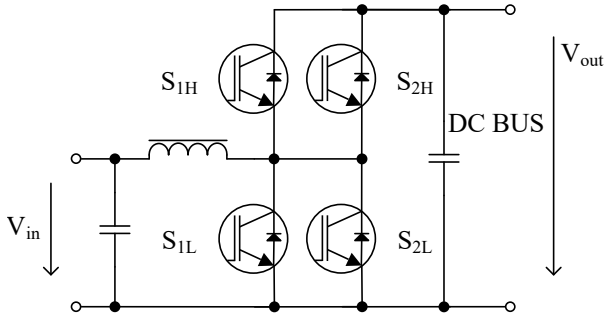

Fig. 1: Boost DC/DC converter for higher power application.

The second option how to share the current is to use the interleaved topology, Fig. 2 [10], [11], [12] and [13]. The same problem as in the previous topology with current sharing is eliminated because the current is divided into two parallel boost converters. The benefits are in improved power density, the interleaved effect reduces the total input and output current ripple, so this means smaller input and output filters (bulk capacitor), better distribution of power with lower current stress for semiconductor devices [3], [4], [5], [6], [7] and [8].

In the high current application, there are used interleaved topologies even with the coupled inductors. The advantage of the coupled inductor is in lowered ripple current through the inductor not only in the output or input current of the converters. The interleaved buck converter with a coupled inductor is used in

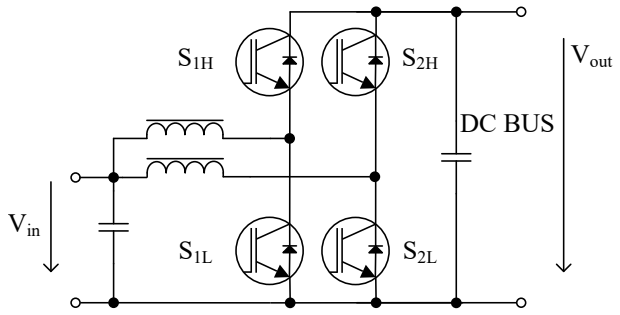

Fig. 2: Interleaved boost DC/DC converter for battery/ultracapacitor application.

VRM application where voltage about 1 V and current of hundreds of amps are applied. On the other side, utilization of coupled inductor in higher voltage application does not have any limitation, as is seen in PFC application [14], [15], [16], [17] and [18]. Therefore, the advantageous features of the coupled inductor will be analyzed for the converter, which serves for boosting voltage from ultracapacitor/battery to DC bus for driving traction motor.

The analysis includes investigation of current ripple - on the input of the converter and change of the inductor current ripple in case of the coupled inductor in comparison with the non-coupled case.

2. Reduction of Current Ripple

The intention of the current ripple reduction in case of battery application is to prolong the battery service life because it is sensitive to high dynamic current stress. Therefore, the boost interleaved topology with reduced input current ripple is proposed to solve this issue. The input of the converter shown in Fig. 2 is connected to battery/ultracapacitor pack and the output to the DC BUS of a three-phase inverter.

This section is divided into two parts. Firstly, an impact of the non-coupled inductor on boost topology is investigated. Then, in some following subheads, the advantage of coupled inductor is analyzed with emphasis on the reduced inductor current ripple.

In the two-phase interleaved converter, the four different operating modes occur, as shown in Fig. 3. The first interval begins when the switches S_{1L} and S_{2H} are closed, the second interval when S_{1H} and S_{2H} are on. In the third interval, S_{2L} and S_{1H} are turn on. It means that the curve of the current i_{L2} in the second phase is same as the current i_{L1} in the first interval but phase-shifted by 180°. Therefore, the ripple of currents in the third interval is same as in the first one (change of current i_{L2} with i_{L1} and vice versa). It can be seen

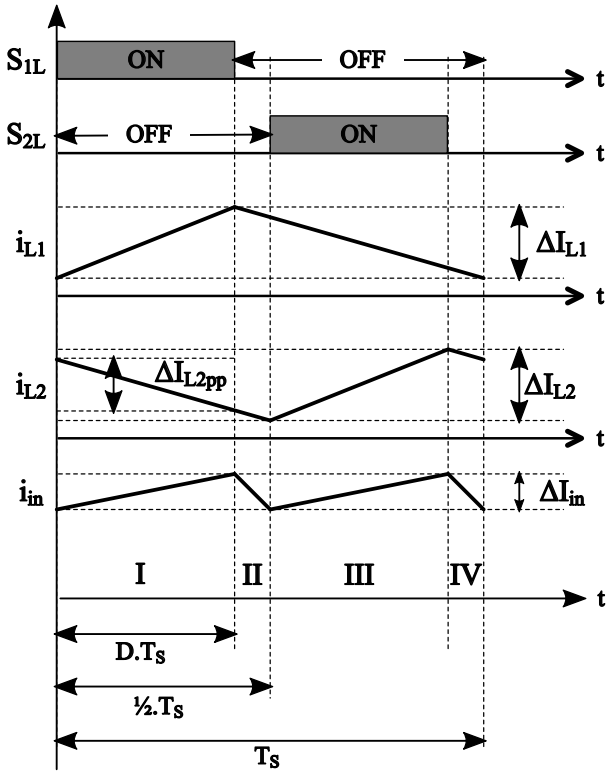

Fig. 3: Current ripples of interleaved non-coupled boost converter.

from the Fig. 3 that ripples ΔI_{L1} and ΔI_{L2} are the same. But, the input current ripple is dependent on ΔI_{L1} and ΔI_{L2pp}, not ΔI_{L2}. Then, appropriate equations for inductor current ripples in the first interval can be obtained, Eq. (1) and Eq. (2).

$$\Delta I_{L1} = \frac{V_{out}}{L}(1-D)DT_S, \tag{1}$$

$$\Delta I_{L2pp} = \frac{V_{in}}{L}(D)DT_S. \tag{2}$$

Then, by summing Eq. (1) and Eq. (2), the equation for input current ripple reduction is:

$$\Delta I_{in} = \Delta I_{L1} + \Delta I_{L2pp} = \frac{V_{out}}{L}(1-2D)DT_S. \tag{3}$$

Using the same procedure, the input current ripple calculation for all intervals can be achieved. On the other hand, in case of the steady state, it is not necessary because the current ripple in all intervals is the same.

2.1. Interleaved Coupled Boost Converter

A simplified schematic for a coupled boost converter is depicted in Fig. 4. The two-phase coupled boost

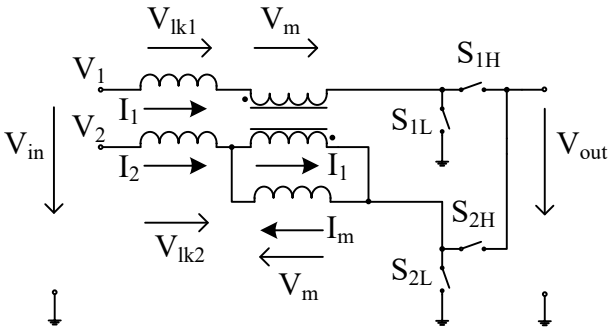

Fig. 4: A simplified schematic of dual interleaved boost converter using coupled inductor.

converter is divided into same four intervals as in the non-coupled case, Fig. 5.

According to Kirchhoff's laws, the following equations for two-phase coupled buck converter in the first interval can be written Eq. (4), Eq. (5), Eq. (6), Eq. (7) and Eq. (8):

$$i_{in} = i_{L1} + i_{L2}, \tag{4}$$

$$i_{in} = i_{L1} - i_{L2}, \tag{5}$$

$$V_{lk1} = V_{in} - V_m, \tag{6}$$

$$V_{lk2} = V_{in} - V_{out} + V_m, \tag{7}$$

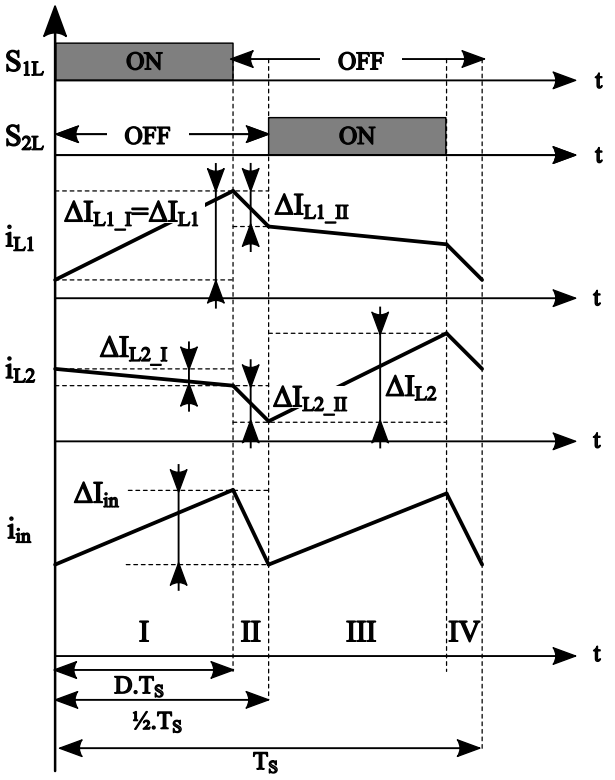

Fig. 5: Current ripples of interleaved coupled boost converter for $D < 0.5$.

$$V_m = \frac{L_m}{L_{lk} + 2L_m} V_{out}. \tag{8}$$

Using the mathematical apparatus, the following equations refer to the first interval of operation Eq. (9), Eq. (10) and Eq. (11):

$$\Delta I_{L1} = \frac{V_{out}}{L_{lk}} \left(1 - D - \frac{L_m}{L_{lk} + 2L_m}\right) DT_S, \tag{9}$$

$$\Delta I_{L2\_I} = \frac{V_{out}}{L_{lk}} \left(\frac{L_m}{L_{lk} + 2L_m} - D\right) DT_S, \tag{10}$$

$$\Delta I_{in} = \Delta I_{L1} + \Delta I_{L2\_I} = \frac{V_{out}}{L_{lk}} (1 - 2D)\, DT_S. \tag{11}$$

These equations also apply for the third interval with the difference that ΔI_{L1} is ΔI_{L2} and vice versa. Using Kirchhoff's laws, the equations for the second interval are as follows, Eq. (12), Eq. (13) and Eq. (14).

$$V_{lk1} = V_{in} - V_{out} - V_m, \tag{12}$$

$$V_{lk2} = V_{in} - V_{out} + V_m, \tag{13}$$

$$V_m = 0. \tag{14}$$

Using the same procedure as in intervals I and III, we can obtain current ripples in intervals II and IV. The given equations are as follows:

$$\Delta I_{L1\_II} = \Delta I_{L1\_II} = \frac{V_{out}}{L_{lk}} (0.5 - D)\, DT_S, \tag{15}$$

$$\Delta I_{in} = \Delta I_{L1\_II} + \Delta I_{L2\_II} = \\ = \frac{V_{out}}{L_{lk}} (1 - 2D)\, DT_S. \tag{16}$$

For the second and fourth interval of operation, the ripple is same for both phase currents. If we want to determine the total inductor current ripple, we must sum the ripple currents in intervals II, III and IV or calculate the ripple in interval I. For the ripple current in the second phase, we can apply the same approach with the difference that we must calculate the ripple in III interval. On the other hand, the input current ripple is the sum of inductor current ripples corresponding to each time interval.

The operation of boost interleaved converter with duty ratio over 0.5 is shown in Fig. 6. It can be seen from this figure that the upper switches of the converter can be switched on at once (interval I and III). It means that in this interval the magnetizing voltage V_m equals zero. Analytically, it is stated in some following equations Eq. (17), Eq. (18), Eq. (19), Eq. (20), Eq. (21) and Eq. (22).

$$V_{lk1} = V_{in} - V_m, \tag{17}$$

$$V_{lk2} = V_{in} + V_m, \tag{18}$$

$$V_m = 0, \tag{19}$$

$$d = D - 0.5, \tag{20}$$

$$\Delta I_{L1\_I} = \Delta I_{L2\_I} = \\ = \frac{V_{out}}{L_{lk}} (1 - D) (D - 0.5) T_S, \tag{21}$$

$$\Delta I_{in} = \Delta I_{L1\_I} + \Delta I_{L2\_I} = \\ = \frac{V_{out}}{L_{lk}} (2 - 2D) (D - 0.5) T_S. \tag{22}$$

Similarly, for the interval II and IV, the following equations apply, Eq. (23), Eq. (24), Eq. (25), Eq. (26), Eq. (27), Eq. (28) and Eq. (29).

$$V_{lk1} = V_{in} - V_m, \tag{23}$$

$$V_{lk2} = V_{in} - V_{out} + V_m, \tag{24}$$

$$V_m = \frac{L_m}{L_{lk} + 2L_m} V_{out}, \tag{25}$$

$$d = 1 - D, \tag{26}$$

$$\Delta I_{L1\_II} = \\ = \frac{V_{out}}{L_{lk}} \left(1 - D - \frac{L_m}{L_{lk} + 2L_m}\right) (1 - D) T_S, \tag{27}$$

$$\Delta I_{L2\_II} = \frac{V_{out}}{L_{lk}} \left(\frac{L_m}{L_{lk} + 2L_m} - D\right) (1 - D) T_S, \tag{28}$$

$$\Delta I_{in} = \Delta I_{L1\_II} + \Delta I_{L2\_II} = \\ = \frac{V_{out}}{L_{lk}} (1 - 2D) (1 - D) T_S. \tag{29}$$

From Eq. (3), Eq. (11) and Eq. (16), it is evident that input current ripple is the same (except the negative sign in Eq. (16)) under the condition that leakage inductance L_{lk} is equaled to non-coupled inductance L. If we substitute the value of duty ratio into the Eq. (22) and Eq. (28), we find that the ripple is same as in the Eq. (3), Eq. (11) and Eq. (16). The condition of $D < 0.5$ for Eq. (22) and $D > 0.5$ for Eq. (28) must be fulfilled.

The coupling coefficient k is the most important parameter which affects inductor current ripple, Eq. (30).

$$k = \frac{L_m}{L_{lk} + L_m}. \tag{30}$$

Using the high value of the coupling coefficient (near 1), the leakage inductance is almost zero. It leads to increasing of the input current ripple ΔI_{in}, but the ripple of the phase current ΔI_{L1} or ΔI_{L2} is minimized. Using the smaller value of k, the magnetizing inductance is smaller and the ripple of the phase current is higher. But, the ripple of the input current is smaller because of higher leakage inductance. Then, the bulky input filter is reduced. Therefore, there is a trade-off in choosing the coupling coefficient.

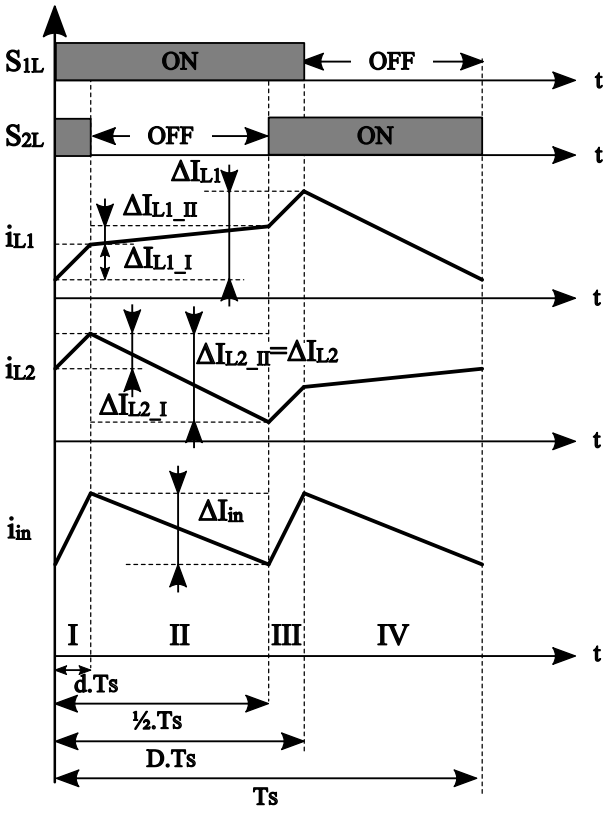

Fig. 6: Current ripples of interleaved coupled buck converter for $D > 0.5$.

3. Simulation Results

As mentioned in section II, the inductor current ripple is strongly dependent on the coupling coefficient k of the coupled inductor. In order to achieve the maximum inductor current ripple reduction, the coupled inductor should have high k and also enough leakage inductance to maintain input current ripple.

The switching frequency of the one leg of the interleaved converter was set to 20 kHz, due to use of the inverter. Therefore, because of the interleaving effect, the switching frequency (input ripple frequency) is doubled, which is shown in Fig. 7, Fig. 8 and Fig. 9. The self-inductance of the non-coupled inductor was set at 370 μH. In order to satisfy the condition of the ripple current equality, the leakage inductance was also set to 370 μH. Then, the coupling coefficient of the proposed coupled inductor has a value of 0.68, resulting in the magnetizing inductance of 784 μH. The additional parameters of the converter are given in Tab. 1. The simulation results are done for duty ratio 34 % (maximum input voltage), 50 % (almost zero current input ripple) and 60 % (minimum input voltage).

The time waveforms of ripple current for the maximum and minimum value of duty cycle are depicted in Fig. 7 and Fig. 8. It is evident from the simulation

Tab. 1: Setup condition.

Parameters	Coupled Inductor	Non-Coupled Inductor
Switching frequency	20 kHz	20 kHz
Leakage inductance	370 µH	-
Magnetizing inductance	784 µH	-
Self-inductance	-	370 µH
Duty cycle	0.34 – 0.6	0.34 – 0.6
Input voltage	150 – 250 V	150 – 250 V
Output voltage	390 V	390 V

results in Fig. 7 and Fig. 8 that the inductor current ripple of the converter with a coupled inductor (i_{L3}, i_{L4}) is smaller than the non-coupled case (i_{L1}, i_{L2}). In Fig. 9, there are given time waveforms of ripple currents for non-coupled (i_{L1}, i_{L2}) and coupled inductor (i_{L3}, i_{L4}) with the difference that the ripple of input current (i_{V1}, i_{V2}) equals almost zero. The advantage is not in zero value of input current because same option occurs in interleaved connection with a non-coupled inductor (50 %), but in the fact that there is reduced inductor current ripple.

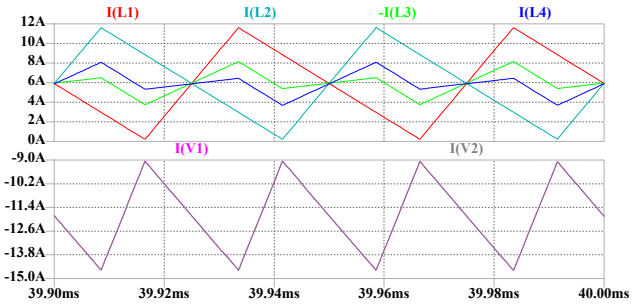

Fig. 7: Inductor current ripples with $D = 34$ % for coupled (I(L3) and I(L4|) and non-coupled inductor (I(L1) and I(L2)) - up, input current ripples for coupled (I(V1)) and non-coupled inductor(I(V2)) - down.

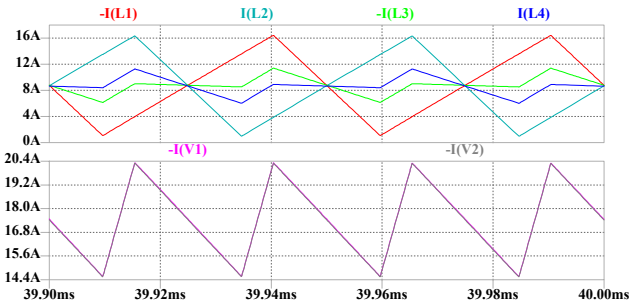

Fig. 8: Inductor current ripples with $D = 60$ % for coupled (I(L3) and I(L4|) and non-coupled inductor (I(L1) and I(L2)) - up, input current ripples for coupled (I(V1)) and non-coupled inductor(I(V2)) - down.

The comparison of the ratio between input and inductor currents is depicted in Fig. 10. It is obvious that the ratio is increased when the coupling effect is utilized. This means that the inductor current ripple is smaller in a whole range of duty cycle except for $D = 0.5$ (ripple is equal). To satisfy the same ripple of the input current for the coupled and non-coupled case, the condition of the same leakage inductance must be met. That means the leakage inductance is same as the self-inductance in non-coupled case.

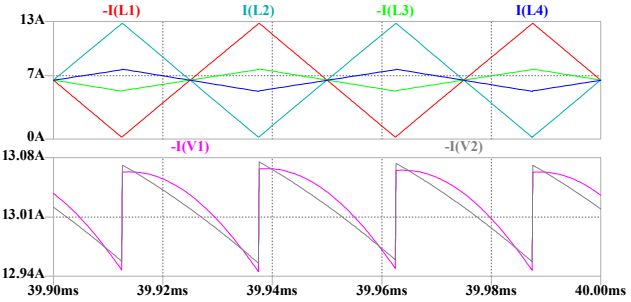

Fig. 9: Inductor current ripples with $D = 50$ % for coupled (I(L3) and I(L4|) and non-coupled inductor (I(L1) and I(L2)) - up, input current ripples for coupled (I(V1)) and non-coupled inductor(I(V2)) - down.

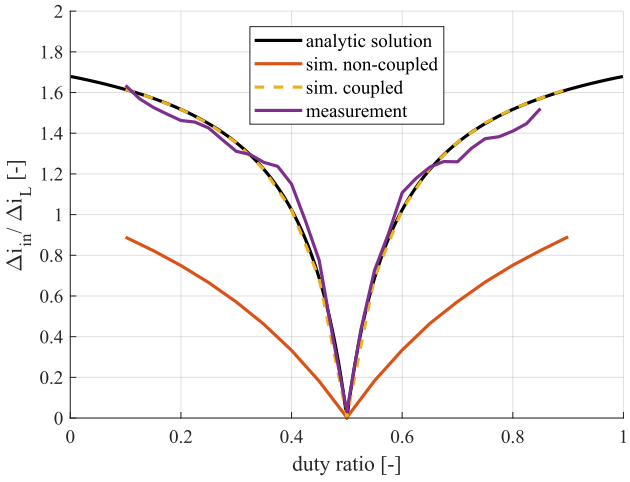

Fig. 10: The ratio of input current ripple and inductor current ripple for analytic solution (coupled), simulation (non- and coupled) and measurement (coupled).

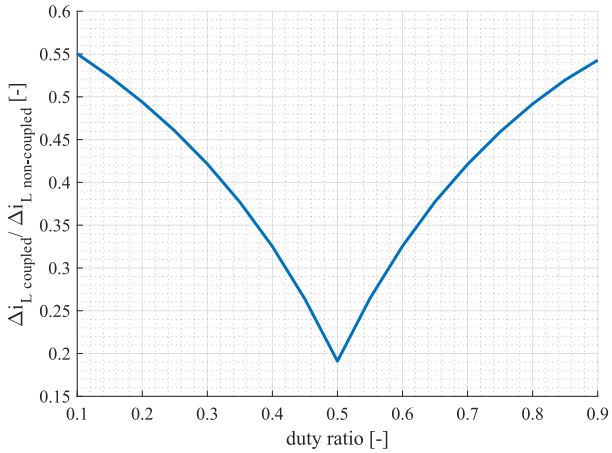

Fig. 11: The ratio of coupled inductor current ripple to non-coupled inductor current ripple.

In contrast with Fig. 10, in Fig. 11, it is seen that there is a ratio of inductor currents, and the ripple of the coupled inductor current is smaller than the non-coupled case in the whole range of duty cycle.

4. Experimental Verification

In coupled inductor design, there should be a problem how to maintain the required leakage inductance. As the easiest way how to manage this issue, the additional non-coupled inductor is used. The powder core is ideal for this inductor, which is capable of carrying high DC current. Then the magnetizing inductance will wound as a coupled inductor, and only the AC component of the current will flow through it because the DC current is canceled with the negative coupling of the inductors. It means that the inductors are wound against each other, and the magnetic flux of both inductors is canceled. Therefore, the solution with the ferrite core should be utilized. The proposed coupled inductor in this paper does not use an additional inductor. The coils consist of two EE cores, where each winding is wound on the outer leg of the core. This ensures a sufficiently large value of inductor leakage, and magnetizing inductance is adjusted by a change of an air gap in the center leg or the outer legs.

The final values of the leakage and magnetizing inductance are given in Tab. 1.

Subsequently, the experimental measurements of the converter with a coupled inductor were performed.

The oscilloscope waveform with the duty lower than 50 % (minimum operating duty ratio - 34 %) is shown in Fig. 12 and with duty higher than 50 % (maximum operating duty ratio - 60 %) in Fig. 13.

In Fig. 12 and Fig. 13, the waveforms of the input and inductor currents with the minimum and maximum operating point of the converter are shown. From

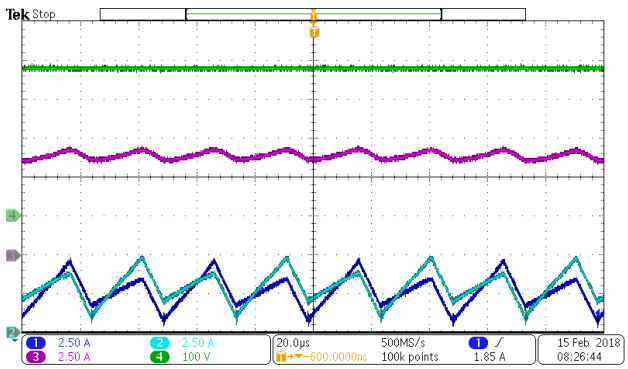

Fig. 12: The time waveforms of inductor current ripple (turquoise and blue one), input current (violet) and input voltage (green) for $D < 0.5, D = 0.34$.

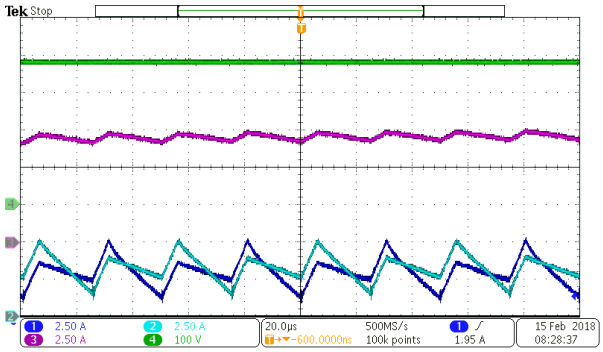

Fig. 13: The time waveforms of inductor current ripple (turquoise and blue one), input current (violet) and input voltage (green) for $D > 0.5$, $D = 0.6$.

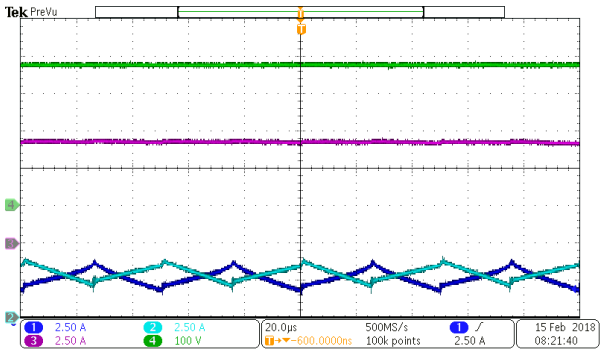

Fig. 14: The time waveforms of inductor current ripple (turquoise and blue one), input current (violet) and input voltage (green) for $D = 0.5$.

Fig. 14, it is visible that the ripple of the input current is markedly reduced which allows to use smaller input capacitor value and extend the lifetime of ultra-capacitor/battery pack connected to the input of the converter.

5. Conclusion

In order to reduce inductor current ripple as well as input current ripple, the two inductors should be coupled to the same core. It is preferable to use coupled inductor topology in battery/ultra capacitor application due to less stress of these energy sources and lower conduction losses of the semiconductor switches because of the lower effective value of the inductor current ripple. To maintain the required ripples on the inductor and on the input, the coupling coefficient must agree. For the output current, the leakage inductance is very important, and it must be equal to the non-coupled inductance to maintain the criterion. Then, for the high value of coupling coefficient, the mutual inductance increases and leakage inductance decreases and vice versa. The solution is to find an appropriate compromise between the output and inductor ripple value.

In the future work, the three and four-phase converters with a coupled inductor will be investigated.

Acknowledgment

This paper is supported by the following project: APVV-15-0571.

References

[1] KIM, S. J. and H. L. DO. Interleaved Flyback Converter with a Lossless Snubber. *International Review of Electrical Engineering (IREE).* 2014, vol. 9, iss. 5, pp. 882–888. ISSN 1827-6660. DOI: 10.15866/iree.v9i5.2800.

[2] AZIB, T., M. BENDALI, C. LAROUCI and K. E. HEMSAS. Fault Tolerant Control of Interleaved Buck Converter for Automotive Application. *International Review of Electrical Engineering (IREE).* 2015, vol. 10, iss. 3, pp. 336–343. ISSN 1827-6660. DOI: 10.15866/iree.v10i3.5472.

[3] TSENG, K. C., J. Z. CHEN, J. T. LIN, C. C. HUANG and T. H. YEN. High Step-up Interleaved Forward-Flyback Boost Converter with Three-Winding Coupled Inductors. *IEEE Transactions on Power Electronics.* 2015, vol. 30, iss. 9, pp. 4696–4703. ISSN 0885-8993. DOI: 10.1109/TPEL.2014.2364292.

[4] HUANG, X., F. C. LEE, Q. LI and W. DU. High-Frequency High-Efficiency GaN-Based Interleaved CRM Bidirectional Buck/Boost Converter with Inverse Coupled Inductor. *IEEE Transactions on Power Electronics.* 2016, vol. 31, iss. 6, pp. 4343–4352. ISSN 0885-8993. DOI: 10.1109/TPEL.2015.2476482.

[5] HU, X., G. DAI, L. WANG and C. GONG. A Three-State Switching Boost Converter Mixed-With Magnetic Coupling and Voltage Multiplier Techniques for High Gain Conversion. *IEEE Transactions on Power Electronics.* 2016, vol. 31, iss. 4, pp. 2991–3001. ISSN 0885-8993. DOI: 10.1109/TPEL.2015.2453634.

[6] LIU, H. and D. ZHANG. Two-Phase Interleaved Inverse-Coupled Inductor Boost without Right Half-Plane Zeros. *IEEE Transactions on Power Electronics.* 2017, vol. 32, iss. 3, pp. 1844–1859. ISSN 0885-8993. DOI: 10.1109/TPEL.2016.2565723.

[7] CHEN, Y. T., Z. X. LU and R. H. LIANG. Analysis and Design of a Novel High-Step-Up DC/DC Converter with Coupled Inductors. *IEEE Transactions on Power Electronics.* 2017, vol. 33, iss. 1, pp. 425–436. ISSN 0885-8993. DOI: 10.1109/TPEL.2017.2668445.

[8] LEE, J. P., H. CHA, D. SHIN and K. J. LEE. Analysis and Design of Coupled Inductors for Two-Phase Interleaved DC-DC Converters. *Journal of Power Electronics.* 2013, vol. 13, iss. 3, pp. 339–348. ISSN 1598-2092. DOI: 10.6113/JPE.2013.13.3.339.

[9] ZIVANOV, M., B. SASIC and M. LAZIC. Desing of Multiphase Boost Converter for Hybrid Fuel Cell/Battery Power Sources. In: *Paths to Sustainable Energy.* Rijeka: InTech, 2010, pp. 359–404. ISBN 978-953-307-401-6.

[10] PERDULAK, J., D. KOVAC, I. KOVACOVA, M. OCILKA, A. GLADYR, D. MAMCHUR, I. ZACHEPA, T. VINCE and J. MOLNAR. Effective utilization of photovoltaic energy using multiphase boost converter in compare with single phase boost converter. *CSL Communications - Scientific letters of university of Zilina.* 2013, vol. 15, iss. 3, pp. 1–6. ISSN 1335-4205.

[11] EBISUMOTO, D., M. ISHIHARA, S. KIMURA, W. MARTINEZ, M. NOAH, M. YAMAMOTO and J. IMAOKA. Design of a four-phase interleaved boost circuit with closed-coupled inductors. In: *Proceedings of the IEEE Energy Conversion Congress and Exposition (ECCE).* Milwaukee: IEEE, 2016, pp. 18–22. ISBN 978-1-5090-0737-0. DOI: 10.1109/ECCE.2016.7855022.

[12] FRIVALDSKY, M., B. HANKO, M. PRAZENICA and J. MORGOS. High Gain Boost Interleaved Converters with Coupled Inductors and with Demagnetizing Circuits. *Energies.* 2018, vol. 11, iss. 1, pp. 1–20. ISSN 1996-1073. DOI: 10.3390/en11010130.

[13] KOSAI, H., S. MCNEAL, A. PAGE, B. JORDAN, J. SCOFIELD and B. RAY. Characterizing the Effects of Inductor Coupling on the Performance of an Interleaved Boost Converter. *IEEE Transactions on Magnetics.* 2009, vol. 45, iss. 10, pp. 4812–4815. ISSN 0018-9464. DOI: 10.1109/TMAG.2009.2024639.

[14] BERES, T., M. OLEJAR and J. DUDRIK. Bidirectional DC/DC converter for hybrid battery. In: *14th International Power Electronics and Motion Control Conference (EPE/PEMC).* Ohrid: IEEE, 2010, pp. 78–81. ISBN 978-1-4244-7856-9. DOI: 10.1109/EPEPEMC.2010.5606617.

[15] KROICS, K., U. SIRMELIS and V. BRAZIS. Design of coupled inductor for interleaved boost converter. *Przeglad Elektrotechniczny.* 2014,

vol. 90, iss. 12, pp. 91–94. ISSN 0033-2097. DOI: 10.12915/pe.2014.12.21.

[16] SPANIK, P., M. FRIVALDSKY, P. DRGONA and J. KUCHTA. Properties of SiC Power Diodes and their Performance Investigation in CCM PFC Boost Converter. In: *17th International Conference on Electrical Drives and Power Electronics EDPE 2013*. Dubrovnik: IEEE, 2013, pp. 22–25. ISBN 978-953-56937-8-9.

[17] DUDRIK, J., P. SPANIK and N. D. TRIP. Zero-Voltage and Zero-Current Switching Full-Bridge; DC Converter With Auxiliary Transformer. *IEEE Transactions on Power Electronics.* 2006, vol. 21, iss. 5, pp. 1328–1335. ISSN 0885–8993. DOI: 10.1109/TPEL.2006.880285.

[18] ESFANDIARI, G., H. ARAN and M. EBRAHIMI. Comprehensive Design of a 100 kW/400 V High Performance AC-DC Converter. *Advances in Electrical and Electronic Engineering.* 2015, vol. 13, iss. 5, pp. 417–429. ISSN 1336-1376. DOI: 10.15598/aeee.v13i5.1313.

About Authors

Slavomir KASCAK was born in Krompachy, Slovakia. He received the M.Sc. degree in power electronics and the D.Sc. degree in automation focused on electrical drives from the Faculty of Electrical Engineering of the University of Zilina, Slovakia, in 2010 and 2013, respectively. He is currently a Researcher and an Assistant Professor in Department of Mechatronics and Electronics. His current research activities include power electronics, electrical drives, and control.

Miriam JARABICOVA was born in Zilina, Slovakia. She received the M.Sc. Degree in Telecommunication focused on telecommunication technics from the Faculty of Electrical Engineering of the University of Zilina, Slovakia in 1999. From 1999 to 2016 she was with Elteco company as a layout engineer specialist. She is currently an internal Ph.D. student at the University of Zilina - Department of Mechatronics and Electronics in the power electrical engineering study program. The main research interest is about power electronic systems.

Michal PRAZENICA was born in 1985 in Zilina (Slovakia). He is graduated from the University of Zilina (2009). He received the Ph.D. degree in Power Electronics from the same university in 2012. He is now Research worker at the Department of Mechatronics and Electronics at the Faculty of Electrical Engineering, University of Zilina. His research interest includes analysis and modeling of power electronic systems, electrical machines, electric drives, and control.

Marek PASKALA was born in 1977 in Nove Zamky. He received the M.Sc. Degree in Mechatronics at Slovak Technical University in Bratislava. After graduation, he was with Slovak Academy of Science as a research worker. From 2005 to now he is as a research worker at the Department of Mechatronics and Electronics, at the University of Zilina. He received the Ph.D. degree in Automation from the same university in 2014. His research interest includes mechatronic systems and control of PLC systems.